INTERNATIONAL JOURNAL OF CLIMATOLOGY
Int. J. Climatol. **38** (Suppl.1): e160–e177 (2018)
Published online 1 December 2017 in Wiley Online Library
(wileyonlinelibrary.com) DOI: 10.1002/joc.5360

Remote SST forcing on Indian summer monsoon extreme years in AGCM experiments

Annalisa Cherchi,[a,b]* Fred Kucharski[c] and Florence Colleoni[a]

[a] *Fondazione Centro Euro-Mediterraneo sui Cambiamenti Climatici, Bologna, Italy*
[b] *Istituto Nazionale di Geofisica e Vulcanologia, Bologna, Italy*
[c] *The Abdus Salam International Centre for Theoretical Physics, Trieste, Italy*

ABSTRACT: An ensemble of AMIP-type experiments with prescribed interannual varying sea surface temperature (SST) and different initial conditions is used to study the relationship between Indian summer monsoon extreme conditions and the El Nino Southern Oscillation (ENSO). Based on the selection of extreme monsoon rainfall years 'In Phase' or 'Out of Phase' with respect to the observations, this study identifies specific SST and atmospheric circulation patterns responsible for the remote forcing on the monsoon. A clear common characteristic of externally forced extreme monsoon years is identified with an ENSO pattern having summer SST anomalies of the same sign in the tropical Pacific Ocean but also in the Indian and Atlantic tropical sectors. This finding assumes that the SST pattern in summer is enough to modulate the Walker circulation and consequently to suppress or enhance convection over South Asia, even if it does not evolve into an ENSO event. The analysis of the 'Out of Phase' cases (i.e. when the model reproduces a weak monsoon instead of a strong one, or the reverse) reveals how the model wrongly responds to the SST forcing, ignoring other processes like ocean–atmosphere coupling. Once ENSO is linearly removed the main source of remote forcing for strong (weak) monsoon characteristics over India is the tropical Atlantic with negative (positive) anomalies, and with weak anomalies of the same sign located in the south Indian Ocean. The results of the role of the forcing from the tropical Atlantic are also confirmed by a set of atmospheric model experiments where interannually varying SST is prescribed only in the Atlantic Ocean, while the rest of the SST is climatological.

KEY WORDS ISM interannual variability; ENSO-monsoon teleconnection; remote forcing; AMIP experiments

Received 3 February 2017; Revised 7 September 2017; Accepted 1 November 2017

1. Introduction

The Indian summer monsoon (ISM) is one of the main sources of water for India, and despite it occurs every year its intensity and basic characteristics can be highly variable from year to year (Webster *et al.,* 1998). One of the dominant remote forcing influencing its variability has been identified in the El Nino Southern Oscillation (ENSO). This remote influence is known since the beginning of the 19th century (Walker, 1924) and it has been widely investigated since then (Sikka, 1980; Rasmusson and Carpenter, 1983; Webster *et al.,* 1998; Kirtman and Shukla, 2000; Kumar *et al.,* 2006, among others). The dynamical teleconnection between ENSO and ISM works through the sea surface temperature (SST) pattern in the Tropical Pacific being able to induce east–west shifts in the Walker circulation that interact with the regional monsoon Hadley circulation (i.e. Webster *et al.,* 1998; Krishnamurthy and Goswami, 2000; Fasullo and Webster, 2002). The east–west displacement of the ascending and descending branches of the Walker circulation links the Indo-Pacific climates with India, that is more prone to drought when the ocean warming signature of El Nino extends westward (Kumar *et al.,* 2006). The ENSO-monsoon relationship and the interaction between Walker circulation and local Hadley cell are tuned by the Indian Ocean dipole (IOD) dynamics (Ashok *et al.,* 2001). In particular, a positive IOD co-occurring with El Nino modulates the meridional circulation inducing anomalous convergence over the Bay of Bengal, reducing the ENSO-induced anomalous subsidence and leading to excessive monsoon rainfall over the monsoon through region (Ashok *et al.,* 2004).

The dependence of the ISM variability on the remote SST forcing from the Pacific Ocean represents a very important aspect of the monsoon for its prediction. In fact, the understanding that anomalous boundary conditions provide potential predictability is the scientific basis for deterministic climate predictions (Charney and Shukla, 1981). Monsoon predictability is indeed a crucial issue as life and economy of million of people depend on its rainfall. Despite the improvements in the simulations of the basic aspects of the monsoon in state of the art coupled models (Sperber *et al.,* 2013), useful monsoon prediction is still a challenge (Webster and Hoyos, 2010; Turner and Annamalai, 2012) because of its complex nature and the diversity of its interactions. In the South Asian monsoon region, both externally forced and internal variability components have been identified to measure the monsoon

* Correspondence to: A. Cherchi, Fondazione Centro Euro-Mediterraneo sui Cambiamenti Climatici/Istituto Nazionale di Geofisica e Vulcanologia, Via Franceschini 31 40128 Bologna, Italy. E-mail: annalisa.cherchi@ingv.it

potential predictability (Shukla, 1981; Singh and Kriplani, 1986; Goswami, 1998; Mohan and Goswami, 2003; Cherchi and Navarra, 2013, among others). Because of the determining role of the internal 'unpredictable' variability component, some studies tried as well to link it to the monsoon intra-seasonal oscillation (Goswami, 1994; Sperber *et al.,* 2000; Goswami and Xavier, 2005).

The ability of state of the art models in reproducing the ENSO-monsoon teleconnection has been investigated in the past in atmospheric-only as well as coupled models frameworks (Shukla, 1984; Fennessy *et al.,* 1994; Sperber and Palmer, 1996; Annamalai and Liu, 2005; Cherchi and Navarra, 2007; Annamalai *et al.,* 2007; Jourdain *et al.,* 2013, among others). Among those studies, there is common consensus that a realistic mean state (i.e. more realistic monsoon climatology) is an important pre-requisite to have a good performance in terms of monsoon-ENSO teleconnection (Sperber, 1999; Lau and Nath, 2000; Annamalai and Liu, 2005). The comparison of the Coupled Model Intercomparison Project - Phase 3 (CMIP3) coupled models performance highlighted that models that best capture the ENSO-monsoon teleconnection are those that correctly simulate the timing and location of SST and diabatic heating anomalies in the equatorial Pacific and the associated changes in the equatorial Walker circulation during El Nino events (Annamalai *et al.,* 2007). A more recent comparison including also the last generation of state of the art coupled models (i.e. CMIP5, Taylor *et al.,* 2011) confirms that the monsoon-ENSO relationship strongly depends on the simulated seasonal cycle of ENSO, and concluded that the performance in CMIP5 has largely improved compared to that of CMIP3 (Jourdain *et al.,* 2013).

The strength of the ENSO-monsoon teleconnection has varied on interdecadal to multidecadal timescales as well with high (low)-inverse correlation in correspondence of an high (low)-amplitude modulation of ENSO variance (Torrence and Webster, 1999; Krishnamurthy and Goswami, 2000), suggesting that the mechanism at the base of the teleconnections could be the same at the different timescales. In terms of the decadal modulation of ENSO, in the last three decades the eastern tropical Pacific has cooled down, while western Pacific has warmed up (Sohn *et al.,* 2013), forming a sort of La Nina-like decadal pattern. This enhanced east–west thermal contrast in the Pacific Ocean has been found to generate the intensification of the Northern Hemisphere summer monsoon (Wang *et al.,* 2013). Still, if ISM is considered alone, the tendency in the last decades is for decreased rainfall over India (Krishnan *et al.,* 2012; Annamalai *et al.,* 2013; Ratna *et al.,* 2016).

The tendency toward a La Nina-like SST pattern has been attributed to the Atlantic warming during the 20th century reducing the warming in the eastern Pacific through a change in the Walker circulation from the 1970s onward (Kucharski *et al.,* 2011), as well as to a phase shift after the mid-1990s in the warm pool mode associated with greenhouse gases increase (Park *et al.,* 2012). However, other arguments emerged in recent years about the role of natural internal variability (Wang *et al.,* 2012; Kosaka and Xie, 2013), the contribution from the stronger Indian Ocean warming (Luo *et al.,* 2012) or the recent warming trend in the Atlantic SST (McGregor *et al.,* 2014) but an exhaustive explanation is still missing.

In recent decades, a weakening in the ENSO-monsoon relationship has been observed (Kumar *et al.,* 1999; Kinter *et al.,* 2002), despite the increased ENSO variance documented since the 1980s (Cobb *et al.,* 2003, 2013; Li *et al.,* 2011). Different hypotheses have been explored for this recent breakdown, including global warming (Kumar *et al.,* 1999), shift in the Walker cell (Collins *et al.,* 2010), changes in the ENSO characteristics (Kumar *et al.,* 2006), influence of the IOD (Ashok *et al.,* 2004), up to the ideas that this weakening could be a consequence of random fluctuations (Gernushov *et al.,* 2001; van Oldenborgh and Burgers, 2005), or of using fixed definitions of seasons (Xavier *et al.,* 2007). Following from the seminal works of Vimont *et al.* (2001, 2003), Krishnamurthy and Krishnamurthy (2014) discussed the assumption that a seasonal footprinting of the SST from the North Pacific to the subtropical Pacific may affect the trade winds modifying the intensity of the Walker circulation over the Pacific and Indian Oceans depending on the phase of the Pacific Decadal Oscillation (PDO; Trenberth and Hurrell, 1994).

Kucharski *et al.* (2007) found that SSTs in the tropical Atlantic that occur contemporaneous to ENSO may counteract the ENSO-induced Indian monsoon rainfall anomalies, contributing to explain the weakening of the ENSO-monsoon anti-correlation. Once ENSO is removed, the ISM is significantly correlated with the south equatorial Atlantic SSTs (Kucharski *et al.,* 2008, 2009a). Recently, many studies have investigated the impact of the tropical Atlantic SSTs on Indian monsoon rainfall in terms of influences on monsoon depressions (Pottapinjara *et al.,* 2014), upper Indian Ocean heat content (Pottapinjara *et al.,* 2016) and atmospheric waves (Yadav, 2017), also in multi-models frameworks, like AMMA-AGCMs (Losada *et al.,* 2010), CMIP3 coupled models (Barimalala *et al.,* 2012) and CMIP5 coupled models (Kucharski and Joshi, 2017).

In the above context, with this study we intend to contribute to the understanding of the ENSO-monsoon relationship with emphasis on the characteristics of the remote forcing using experiments with atmospheric general circulation models (AGCM) where SST is prescribed (AMIP-type, following from Atmospheric Model Intercomparison Project). Doing this, implications of the role of other remote forcing from the Indian and Atlantic Oceans are also discussed.

AGCM experiments do not perform better than coupled model experiments in reproducing the monsoon-ENSO relationship despite the mean state biases of state of the art coupled model (Sperber *et al.,* 2013; Prodhomme *et al.,* 2015). Still, in this study we have chosen to use AMIP-type experiments because we want to explore further the role of remote SST patterns on ISM extreme years. In fact, our approach consists in selecting strong and weak monsoon years in an ensemble of eight AMIP experiments sharing the same SST and sea-ice boundary conditions taken from

Table 1. List of strong and weak monsoon years in the period 1948–2012 as classified from the observed AIR index (IITM web-site) and in terms of the ISM index for each AMIP member (from #1 to #8), as described in Section 2.3. For each member, strong and weak monsoon years when 'In Phase' with the observed index are highlighted in bold.

	Strong monsoon years	Weak monsoon years
AIR (IITM web-site)	1956 1959 1961 1970 1975 1983 1988 1994	1951 1965 1966 1968 1972 1974 1979 1982 1985 1986 1987 2002 2004 2009
AMIP #1	1949 1955 1958 1962 1964 **1970** 1976 1978 1979 **1983**	1963 **1966** 1973 **1982** **1987** 1991 1993 1997 **2002** **2009**
AMIP #2	1958 **1959** **1961** 1963 1967 1971 1976 1978 1979 2012	1949 **1985** **1986** **1987** 1990 1991 1994 1995 **2002** 2006
AMIP #3	1954 1955 1958 1960 **1961** 1964 1966 1974 1979 1980 1981 **1988**	1948 1984 **1987** 1991 1993 1994 1995 1997 **2009**
AMIP #4	1954 1955 **1956** 1958 1962 **1970** 1974 1978 1980 1981 1989 2010	**1982** **1987** 1990 1993 1995 1997 **2002** 2006 **2009**
AMIP #5	1955 1958 1960 1962 1964 **1970** 1978 1981	1948 1953 **1965** **1966** 1984 **1985** **1987** 1990 1991 1994 1995 1997 2006 2012
AMIP #6	1958 1960 **1961** 1964 1967 1971 **1975** 1979 1982 2003 2011	1957 1963 1969 **1987** 1991 1996 2001 2012
AMIP #7	1950 1955 1958 1960 **1961** 1967 1976 1978 1980 1981 1984 **1988** 2010	1954 **1965** 1969 **1972** **1987** 1989 1990 1991 1993 1994 1995 1996 2001 **2002** 2012
AMIP #8	1954 **1956** 1957 1958 1959 1960 **1961** **1970** 1974 1975 1976 1978	1953 **1986** **1987** 1989 1990 1991 1993 1995 1996 **2002** **2009**

the Hadley Center sea Ice and Sea Surface Temperature (HadISST) data set (Rayner *et al.,* 2003) for the period 1948–2012 and with different initial conditions. At first, these years are grouped and compared with observations and re-analyses in terms of main characteristics of strong and weak monsoons. For each member, the model index may peak in the same years as in the observations but also in others. According to this, another classification is performed by selecting years where the model index peaks in the same years as in the observations and years where the indices peaks are exactly opposite (i.e. in the observations that year is classified as strong, but in the model it results as a weak one) thus building 'In Phase' and 'Out of Phase' groups. Considering the eight members available, relative large samples of cases can be built. A similar approach has been applied to the precipitation over south-eastern South America and the remote SST forcing (mainly from the Pacific Ocean) on it, providing interesting results (Cherchi *et al.,* 2014). In this study, the comparison of years according to the correspondence between monsoon intensities in the model and in the observations provides useful information on the origin of remote SST forcing on ISM precipitation, as well as implications on the role of the other basins (i.e. Indian and Atlantic Oceans). It could well provide clues about the fact that ocean–atmosphere coupling is essential in the warm Indian Ocean.

The study is organized as follows: Section 2 describes the experiments used and the data sets/re-analyses considered for comparison, including the details of the method applied in the selection of the years to build the composites. Section 3 deals with the comparison between AMIP experiments and observations in terms of the characteristics of strong and weak monsoon years. Section 4 is dedicated to specific years selected according to the classification of strong- and weak-simulated monsoon years with common characteristics among the ensemble members and to the discussion of non-ENSO forcing, linearly removing the impact of ENSO and showing results from AMIP experiments with the interannual variability of the SST only in the Atlantic Ocean. Finally, Section 5 collects the main conclusions of the study.

2. Experiments, observed data sets and method of analysis

2.1. AMIP experiments

The ensemble of AMIP experiments used in this study has been performed with the ECHAM4 model (Roeckner *et al.,* 1996) at T106 horizontal resolution. It consists of eight members with same interannually varying SST and sea-ice from 1948 to 2012 derived from the HadISST data set (Rayner *et al.,* 2003) and different initial conditions. The performance of this set of experiments in simulating the mean behaviour of the ISM and some characteristics of its variability has been analysed in Cherchi and Navarra (2013).

2.2. Re-analyses and observed data sets

Precipitation and atmospheric circulation patterns during strong and weak monsoon years simulated in the AMIP experiments have been compared with observed data sets and atmospheric re-analyses. In particular, observed precipitation is taken from the Climate Research Unit (CRU) data set (Mitchell and Jones, 2005), while other atmospheric variables, like wind and velocity potential, are taken from the National Center for Environmental Predictions/National Center for Atmospheric Research (NCEP/NCAR) re-analysis (Kalnay *et al.,* 1996).

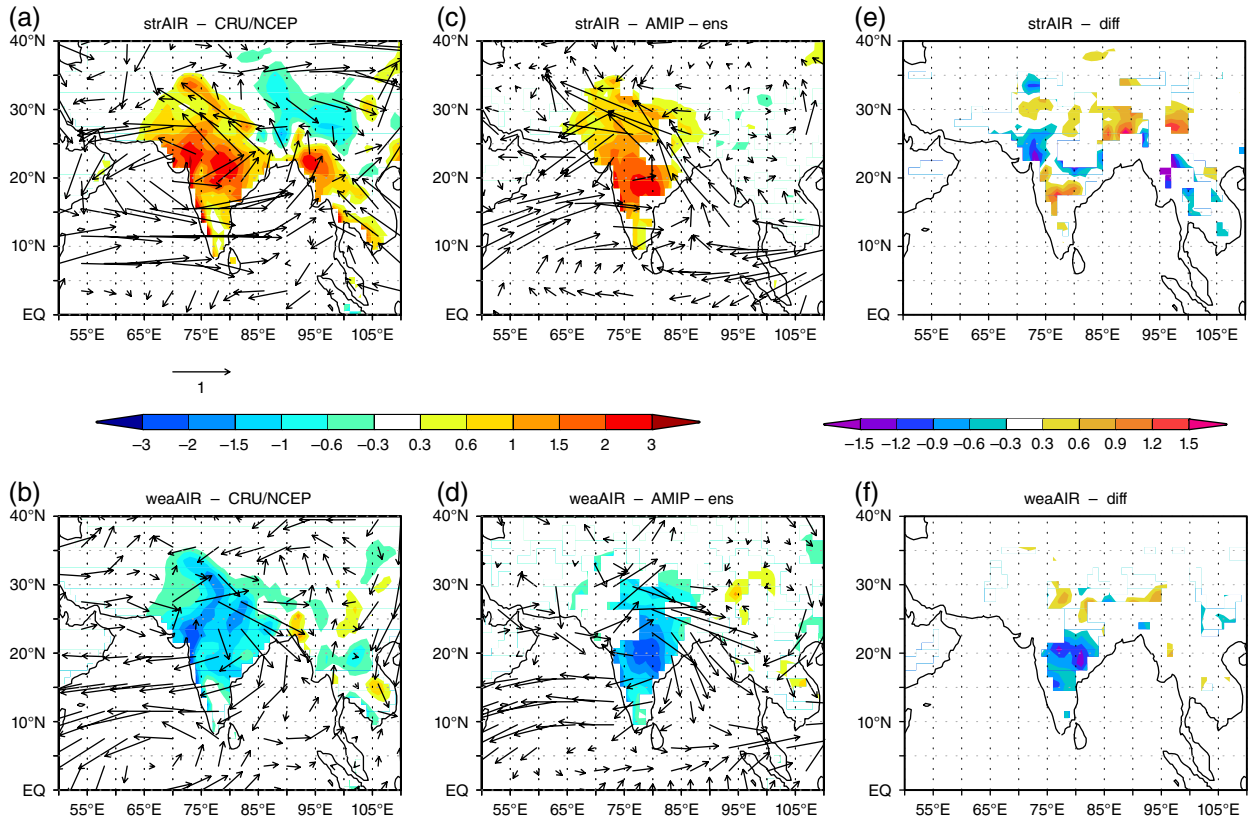

Figure 1. Strong and weak monsoon years composite of precipitation (mm/day, shaded) and 850 hPa wind ($m\,s^{-1}$, vectors) anomalies in (a, b) CRU/NCEP and (c, d) AMIP-ensemble, respectively. (e, f) Differences (model minus observations) of precipitation (mm/day) composite anomalies for strong and weak monsoon years, respectively. For the model, only the values statistically significant at 95% are shown.

2.3. Selection of strong and weak monsoon years and analysis of composites

The whole study is based on the comparison between strong and weak ISM characteristics, where summer refers to the June–September (JJAS) mean. At first, strong and weak monsoon years are classified based on precipitation indices over India. In particular, in the observations strong and weak ISM years are selected based on the All-India Rainfall (AIR) index (averaged in JJAS) defined by Parthasarathy *et al.* (1992) and available from the Indian Institute of Tropical Meteorology (IITM) website (ftp://www.tropmet.res.in/pub/data/rain/iitm-regionrf.txt). The years considered in the analysis are listed in Table 1. In the AMIP experiments, strong and weak ISM years are selected based on JJAS precipitation anomalies averaged over India (land points in the region 70°–90°E, 10°–30°N), mimicking the AIR observed index. In the model, a monsoon year is defined strong (weak) when the standardized precipitation index exceeds 1 (−1) standard deviation. The years selected in each member of the AMIP ensemble are listed as well in Table 1. These years are used to build the composites shown in Figures 1 and 2 for a first comparison between model and observations. To mask the signal of the internal variability from the AMIP experiments the composites shown in Figures 1 and 2 consider all the members (not the ensemble mean).

In the AMIP ensemble, the monsoon precipitation index computed for each member can be compared with the observed AIR index. The correspondence between observed and simulated index is not univocal, but from Table 1 it is possible to identify years when the model index peaks in the same year as in the observations. According to that for each member we have classified years as ‘In Phase’ when the modelled and observed extreme years correspond. These years are highlighted in bold in Table 1. Considering the sign and the intensity of the monsoon index for each member and each year it is possible to identify years having the simulated index of sign opposite to the observed index but with a comparable intensity, i.e. in absolute value higher than 1 standard deviation (not shown). All these years are classified as ‘Out of Phase’ and they are listed in Table 2 for each member of the AMIP ensemble. Simulated ‘In Phase’ and ‘Out of Phase’ years are used to build the composites shown in Figures 3, 4 and 5. This kind of analysis permits to evidence the characteristics in common with (diversified from) the observations that may force strong or weak simulated monsoon years.

Looking at Table 1 (years in bold) and at Table 2 it is evident that some ‘In Phase’ or ‘Out of Phase’ years are common to many members, indicating that they should contain predictability signature. So, for each ‘In Phase’ and ‘Out of Phase’ simulated year listed in Tables 1 and 2,

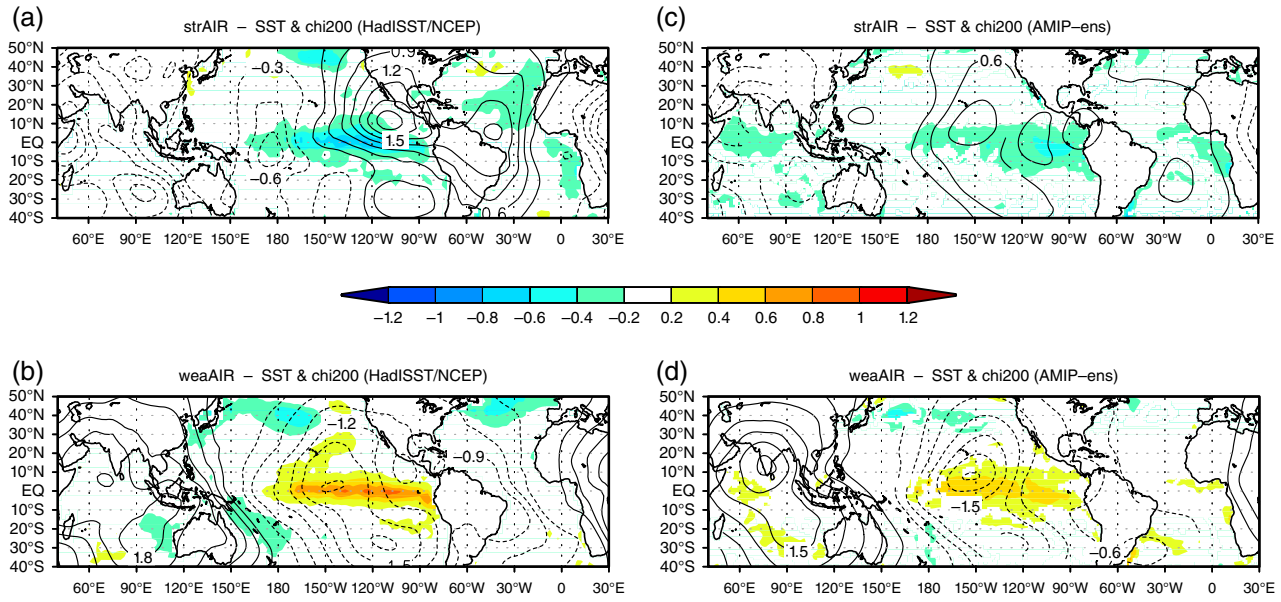

Figure 2. Strong and weak monsoon years composite of SST (K, shaded) and 200 hPa velocity potential ($*10^{-6}$ s^{-2}, contours) anomalies in (a, b) HadISST/NCEP and (c, d) AMIP-ensemble, respectively. For the model, only the values statistically significant at 95% are shown.

Table 2. List of simulated strong and weak monsoon years classified as 'Out of Phase'. As described in Section 2.3, in those years the value of the monsoon index in the model has sign and intensity opposite to the observed index.

	Strong monsoon years 'Out of Phase'	Weak monsoon years 'Out of Phase'
AMIP #1		1951 1972 1974 1979
AMIP #2	1970 1994	1979 1982 2004
AMIP #3	1956 1994	1951 1966 1974 1979 1985 1986 2004
AMIP #4	1983 1994	1966 1968 1974
AMIP #5	1994	1972 1974 1979 1982 2002
AMIP #6	1983 1994	1979 1982
AMIP #7	1994	
AMIP #8	1983	1951 1965 1966 1974

we have identified them as 'common In Phase' and 'common Out of Phase' if at least half of the members agreed in the classification. These years are listed in Table 3 and they are used to build the composites shown in Figures 6 and 7. For example, 1987 is a weak monsoon year in all the member and it is 'In Phase' with the observations, while 1994 is a strong monsoon year 'Out of Phase' with the observations, i.e. meaning that in the model it is a weak monsoon year in almost all the members. These two examples contain interesting information in terms of predictability, in fact 1987 is an El Nino year and 1994 is a positive IOD year. Because of the nature of the experiments used, the comparison of those specific years permits to evidence the common characteristics of the SST forcing or to suggest the role of other factors involved. This is a novelty of our approach that to the best of our knowledge has never been applied to Indian monsoon variability issues.

Table 3 includes also another category of years, identified as 'AMIP-only' because they are extreme monsoon years, either strong or weak, in at least half of the AMIP members but not in the observations. These years are used to build the composites shown in Figure 8.

A non-parametric statistical significance test using Monte Carlo re-sampling techniques (Wilks, 1995) is applied to the composites from the model and only the values statistically significant at 95% are shown in the corresponding figures.

2.4. Non-ENSO forcing

To further investigate on the remote forcing from the other basins (non-ENSO), we have computed new variables (FLDres) linearly removing the ENSO impact as:

$$\mathrm{FLDres} = \mathrm{FLD} - \mathrm{NINO34} * \mathrm{bFLD} \qquad (1)$$

where FLD is the original variable (anomalies), NINO34 is the SST index averaged over the Nino3.4 area (i.e. 170°–120°W, 5°S–5°N) and bFLD is the linear regression coefficient corresponding to the field considered (Kucharski *et al.,* 2008). These regressed fields and the associated new composites (extreme monsoon years are selected based on indices computed from the residual precipitation fields) are shown in Figure 9.

Fully removing ENSO from observations or AMIP experiments with linear regression is a complex task (Compo and Sardeshmukh, 2010), so we complemented the analysis of non-ENSO forcing with two sets of AMIP experiments performed with the SPEEDY atmospheric model (Kucharski *et al.,* 2013) with interannually varying SST in the global ocean (SPEEDY-AMIP) and in the Atlantic Ocean only (SPEEDY-AMIP-ATL). The two sets of experiments are ensemble of seven and four members, respectively, with same SST boundary conditions

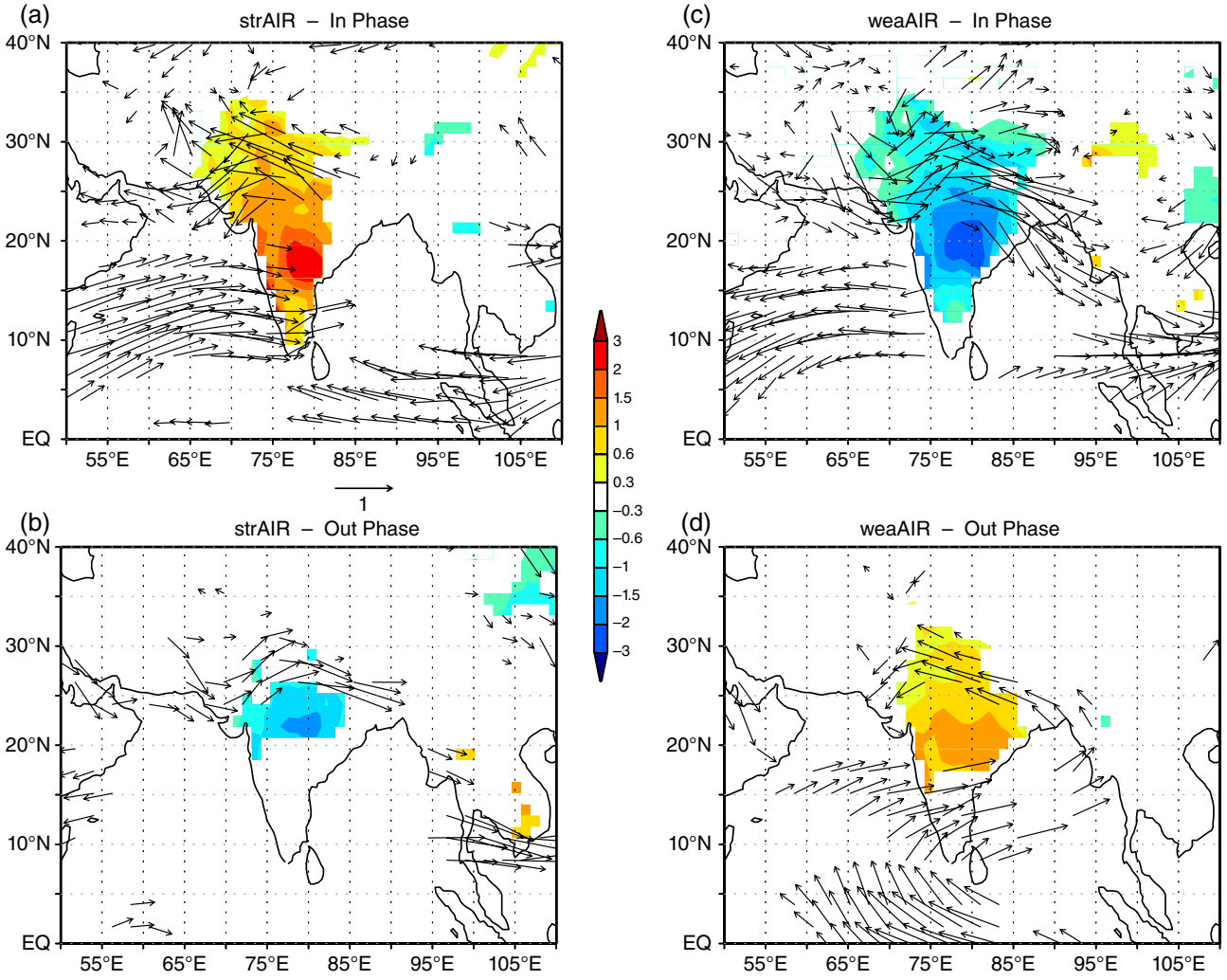

Figure 3. Strong and weak monsoon years composite of precipitation (mm/day, shaded) and 850 hPa winds ($m\,s^{-1}$, vectors) anomalies in AMIP members when the simulated ISM index is (a, c) 'In Phase' and (b, d) 'Out of Phase' with the observed AIR index. See Table 1 (years in bold) and 2 for the years used to build the composites. All the values shown are statistically significant at 95%.

taken from HadISST (Rayner *et al.,* 2003) and different initial conditions. SPEEDY is an atmospheric model of intermediate complexity using simplified physical parameterizations. It is based on a hydrostatic spectral dynamical core. The parameterized processes include short- and long-wave radiation, large-scale condensation, convection, surface fluxes of momentum, heat and moisture, and vertical diffusion. In this study, the AGCM is configured with eight vertical (sigma) levels and with a spectral resolution of T30. The results for strong and weak monsoon composite computed from the two SPEEDY ensembles are shown in Figure 10.

3. Strong and weak monsoon years: Comparing model experiments and observations

The main characteristics of strong and weak monsoon summers are analysed in terms of wind and precipitation. Figure 1 shows the composite anomalies of precipitation and 850 hPa wind anomalies averaged in summer (JJAS) for strong and weak monsoon years. In the AMIP experiments, strong monsoon summers are characterized by intense precipitation in the Indian subcontinent with maxima in the Western Ghats and in the eastern areas, in agreement with the observations (Figures 1(a) and (c)). South of 20°N and north of 27°N, the simulated excessive rainfall is overestimated (Figure 1e). In the eastern part of the Asian continent (i.e. between 87°E and 103°E over South China, Bangladesh, Bhutan, eastern India and Myanmar), there is a strong north–south dipole of precipitation (Figure 1(a)) that is not simulated in the AMIP experiments (Figure 1(c)). The precipitation composite is more symmetric in AMIP experiments than in the observations with mainly one mode of variability over central India (20°N), likely reflecting the wet bias of ECHAM4 over the area when in forced mode (Prodhomme *et al.,* 2014).

The winds at 850 hPa are characterized by a strong south-westerly flow forming in the Indian Ocean and expanding into the continent. In the AMIP experiments, the flow has a stronger meridional component, but it is well captured in terms of intensity (Figures 1(a) and

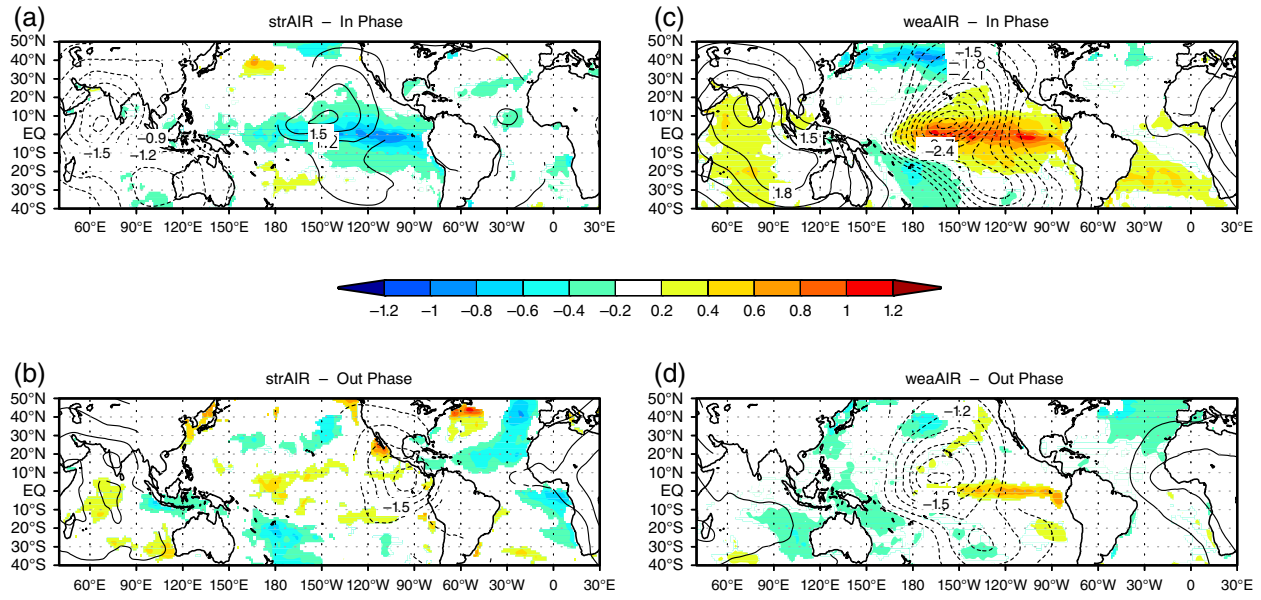

Figure 4. Strong and weak monsoon years composite of SST (K, shaded) and 200 hPa velocity potential (*10^{-6} s^{-2}, contours) anomalies in AMIP members when the simulated ISM index is (a, c) 'In Phase' and (b, d) 'Out of Phase' with the observed AIR index. See Table 1 (years in bold) and 2 for the years used to build the composites. All the values shown are statistically significant at 95%.

(c)). In weak monsoon summers, the surface flow is mostly easterly and it is characterized by a stronger zonal component rather a meridional one, consistently with the NCEP re-analysis (Figures 1(b) and (d)). In the AMIP experiments, the precipitation pattern during weak monsoon years is almost opposite to strong monsoon cases (Figure 1(d)), while in the CRU data set the largest decrease is mostly in the Western Ghats and in the northern part of the subcontinent (Figure 1(b)). In the model, the deficit of precipitation is overestimated, mostly in central India (Figure 1(f)). The dipole described for strong monsoon cases in the eastern part of the Asian continent (i.e. between 87°E and 103°E) is not observed during weak monsoon years, neither with opposite sign (Figure 1(b)). Rather it seems that in the region the anomalies have the same sign of strong monsoon years but with weaker intensity.

To investigate the remote SST response and the associated ENSO-monsoon connection, Figure 2 shows the anomalies of SST and of velocity potential at 200 hPa, representing the modulation of the Walker circulation, for strong and weak monsoon years' composites. AMIP experiments are prescribed with HadISST sea surface temperatures, but in Figure 2 SSTs in the model and in the observations are not the same because strong and weak monsoon years used to build the composite do not exactly correspond (Table 1). In the AMIP experiments, the SST pattern is coherent with observations in the equatorial region, specifically in the eastern Pacific and eastern Atlantic, while the structure in the extra-tropics (i.e. in the North Pacific and North Atlantic) differs (Figure 2). For both strong and weak monsoons, the years selected in the AMIP experiments are characterized by negative and positive anomalies, respectively, also in the tropical Indian Ocean but this is not observed (Figure 2), possibly related with the excessive mean and variability of rainfall over central India characteristic of this AGCM (Prodhomme *et al.,* 2014). In both model and observations, there is a clear symmetry between strong and weak monsoon years, mostly in the equatorial Pacific. The 200 hPa velocity potential is quite symmetric in the AMIP experiments comparing strong and weak monsoon summers (Figures 2(c) and (d)) and the simulated pattern is more similar to observations for weak than for strong monsoon composites (Figure 2), as in the latter case the negative anomalies in the central Pacific are not reproduced. Over India the clear symmetry of upper tropospheric velocity potential could as well be related to the excessive mean and variability of rainfall of the atmospheric model (Prodhomme *et al.,* 2014). The monsoon in the model seems sensible to Pacific SST anomalies with a broader latitudinal extent compared to re-analyses (Figure 2).

As described in Section 2.3, for each member of the ensemble we check whether observed years with strong or weak monsoon are reproduced or not. In a previous analysis of the same set of experiments, we investigated the potential predictability of some monsoon indices, identifying high-predictable years (i.e. with all members converging) associated with ENSO events (Cherchi and Navarra, 2013). Here, we can explore the argument further because the identification of 'In Phase' and 'Out of Phase' groups, as defined in Section 2.3, helps in understanding the role of remote forcing on the simulations of the ISM precipitation and associated atmospheric circulation. A different response in terms of circulation and precipitation to the same SST patterns may be explained by the forced dynamics involved, by the lack of ocean–atmosphere coupling processes, if essential, and also by model biases.

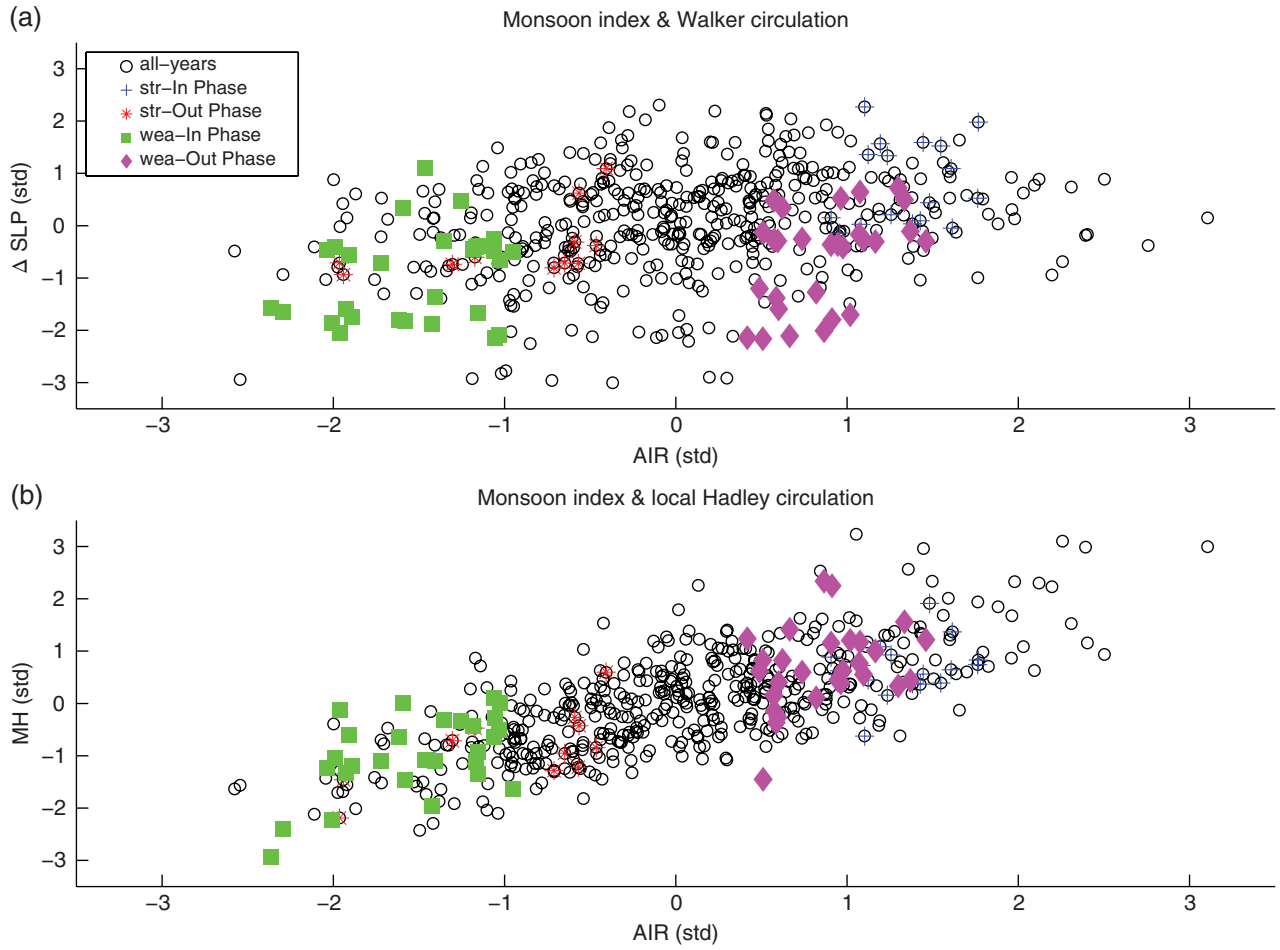

Figure 5. Scatter plots of standardized precipitation index (*x*-axis) *versus* (a) Walker circulation, in terms of ΔSLP standardized index, and (b) local Hadley circulation, in terms of standardized meridional wind shear index, in all AMIP members (black open circles). In each panel, strong 'In Phase' (blue plus signs) and 'Out of Phase' (red asterisks) as well as weak 'In Phase' (green filled squares) and 'Out of Phase' (magenta filled diamonds) years are highlighted.

Table 3. List of years grouped as 'common In Phase', 'common Out of Phase' or 'AMIP-only' for both strong and weak monsoon cases. The number of members involved is indicated in brackets for each case. These 'common' cases are selected, as described in Section 2.3, because at least half of the members agree in the sign and intensity of the index.

	In Phase	Out of Phase	AMIP-only
Strong monsoon	1961(5) 1970(4)	1994(6)	1955(5) 1958(8) 1978(6)
Weak monsoon	1987(8) 2002(5) 2009(4)	1974(5) 1979(5)	1990(5) 1991(6) 1993(5) 1995(6)

Figure 3 shows the anomalies of precipitation and lower troposphere winds in composites of years built considering four cases: monsoons years, either strong or weak, where model and observations agree ('In Phase') and monsoon years either strong or weak in the observations but not in the model ('Out of Phase'). 'In Phase' composites are built considering all the years highlighted in bold in Table 1, while the 'Out of Phase' composites consider the years listed in Table 2. In the cases where the simulated ISM monsoon index agree with the observed index (i.e. 'In Phase' composite), during strong monsoon years the intensity of monsoon precipitation is large in the Western Ghats and in the eastern part of the subcontinent, as described before for the observations, and strong south-westerly winds blow from the Indian Ocean and the Bay of Bengal into the Indian subcontinent (Figure 3(a)). Considering the comparison discussed in Figure 1, it is clear that when we consider exactly the years where simulated and observed ISM indices correspond, the composite is clearly in agreement with the observations, at least over India and adjacent oceans. Same conclusions can be drawn for the cases when model and observations agree in the identification of weak monsoon years, having negative precipitation anomalies over India and strong easterly wind anomalies over the Arabian Sea (Figure 3(c)). The patterns in these strong and weak 'In Phase' composites are almost symmetric (Figures 3(a) and (c)).

On the other hand, when considering the years when in the model the monsoon index has a sign opposite to what

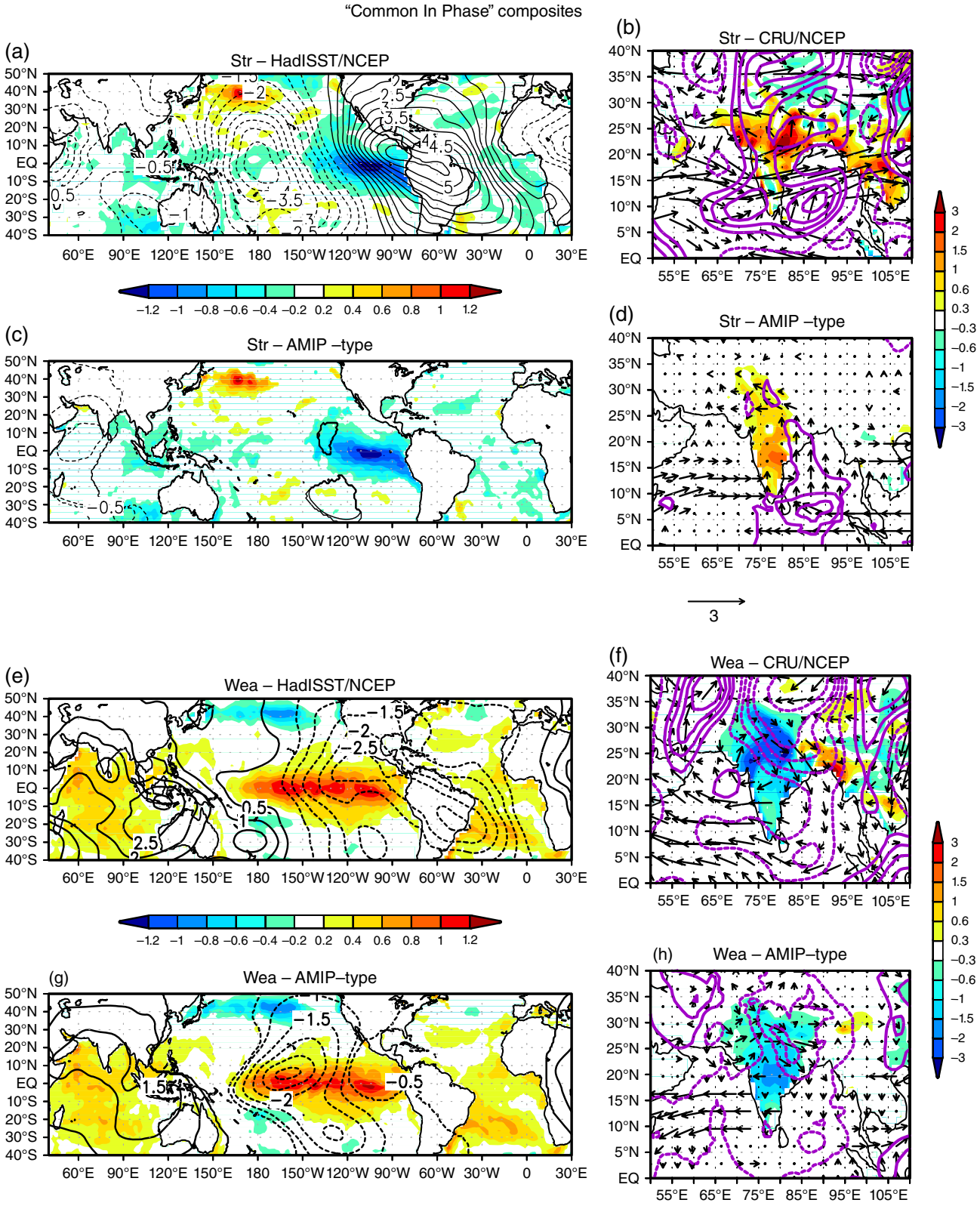

Figure 6. Anomalies of (a, c) SST (K, shaded) and velocity potential (*10^{-6} s^{-2}, contours) at 200 hPa and of (b, d) precipitation (mm/day, shaded), 850 hPa winds (m s^{-1}, vectors) and meridional wind shear (m s^{-1}, purple contours) for strong monsoon years composite classified as 'common In Phase' in the re-analyses/observations and in the AMIP members, respectively. (e, g) same as (a, c) and (f, h) same as (b, d) but for weak monsoon years. The years included in the classification are listed in Table 3 (second column). For the model, only the values statistically significant at 95% are shown.

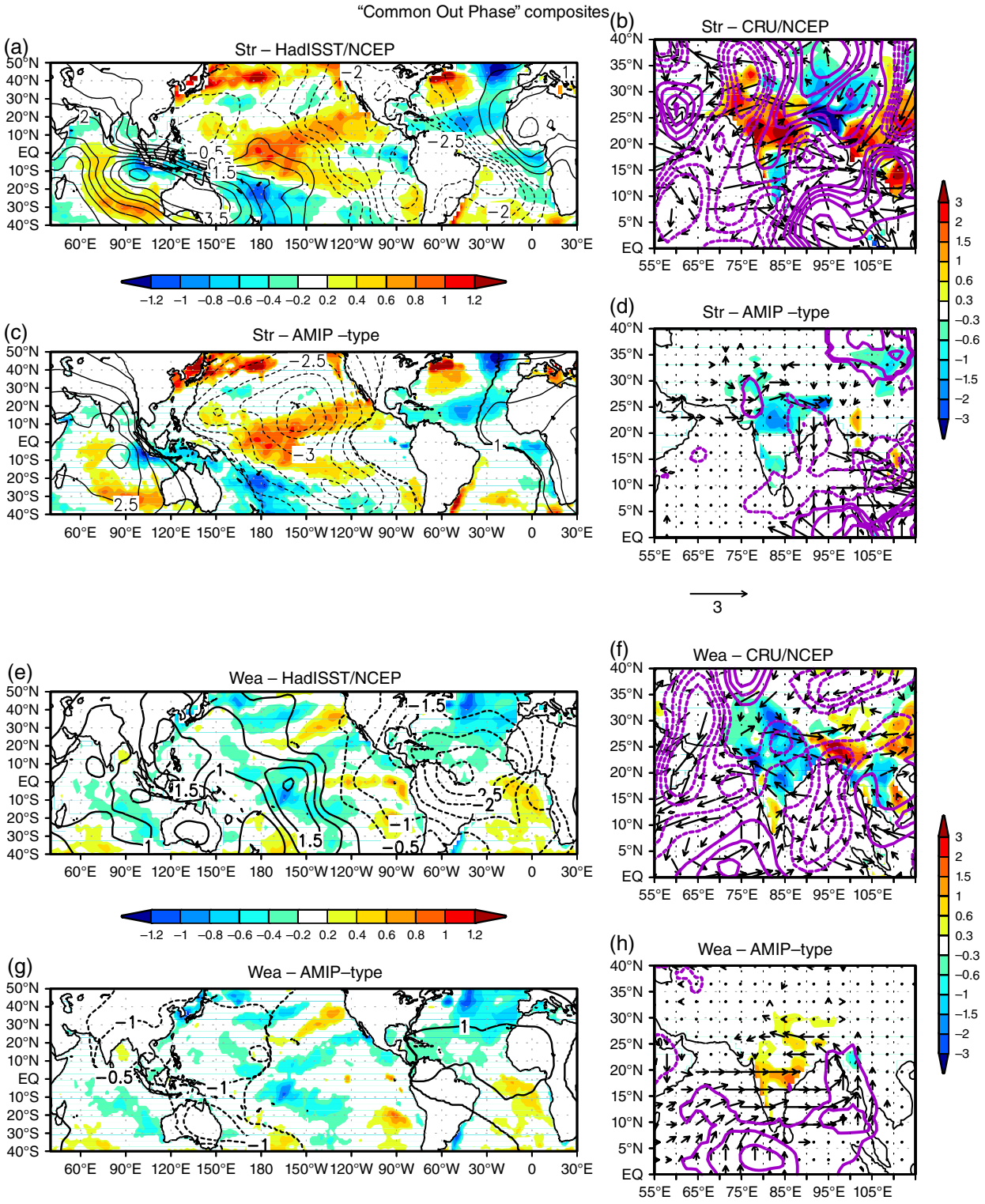

Figure 7. Same as Figure 6 but for strong and weak monsoon years composites classified as 'common Out of Phase'. The years included in the classification are listed in Table 3 (third column). For the model, only the values statistically significant at 95% are shown.

observed and with comparable intensity ('Out of Phase' cases), the composites (Figures 3(b) and (d)) reveal the characteristics of the opposite phase of the monsoon. In fact, Figures 3(b) and (d) is similar to Figures 3(a) and (c) either in terms of sign and intensity of the anomalies, but with some differences as the precipitation maximizes mostly in the central part of the subcontinent. In terms of winds, especially in the weak 'Out of Phase' case (Figure 3(d)), the flow has a larger southerly component confined east of 65°E and entering the continent mostly from south, compared to the strong 'In Phase' composite (Figure 3(a)).

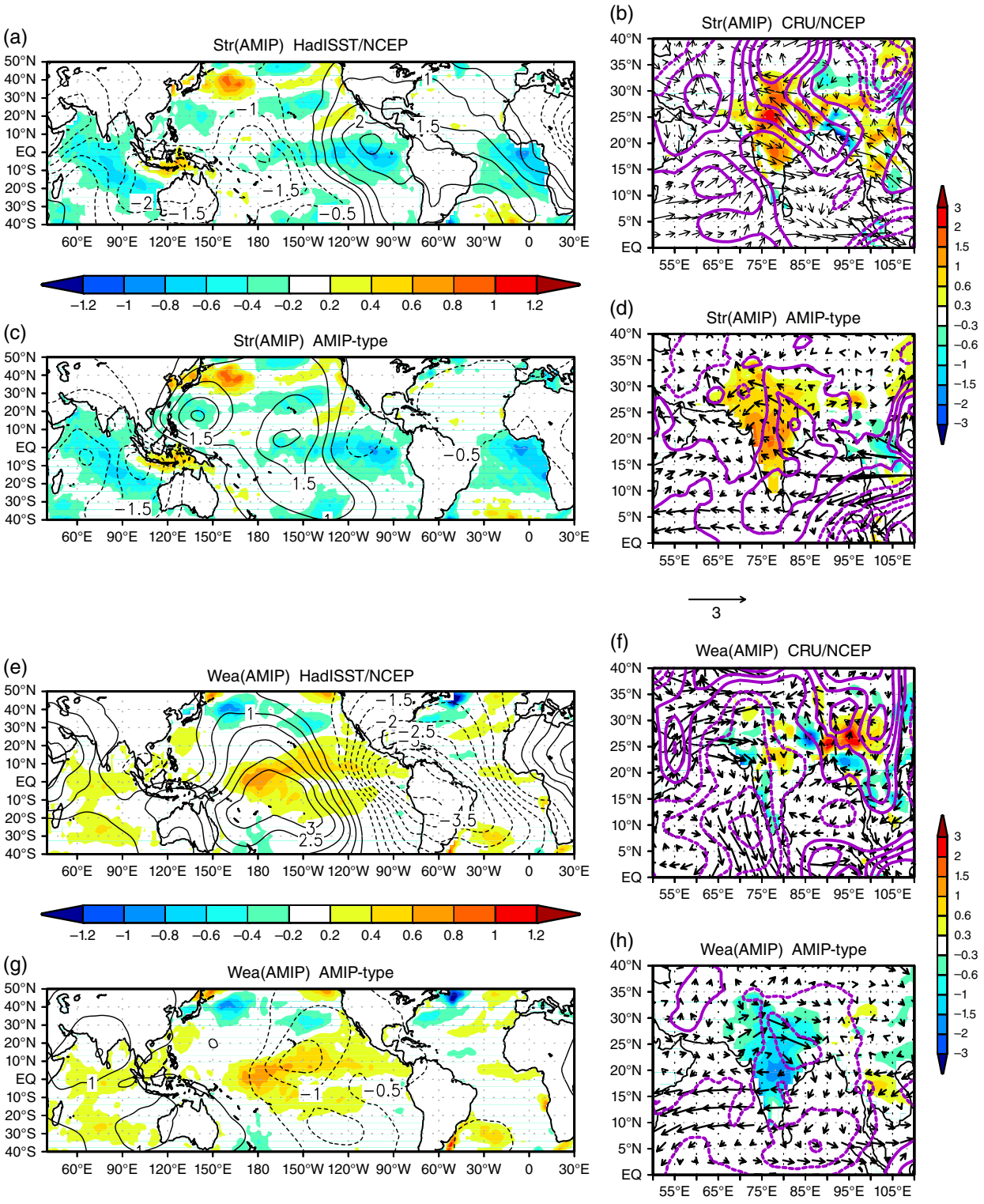

Figure 8. Same as Figure 6 but for strong and weak monsoon years in 'AMIP-only' composites. The years included in the classification are listed in Table 3 (fourth column). For the model, only the values statistically significant at 95% are shown.

Figure 4 shows the composite anomalies of SST and upper tropospheric velocity potential for the same cases of Figure 3: the comparison with Figure 2 should indicate which remote SST condition is mostly favourable for strong or weak monsoon precipitation over India and associated atmospheric circulation. Starting with the group 'In Phase', where simulated extreme monsoon years coincide with the observed one, SST and velocity potential patterns are almost symmetric in strong and weak monsoon years (Figures 4(a) and (c)). As expected, in these cases the SST pattern is clearly in ENSO phase with an eastern equatorial Pacific anomalously cold when the monsoon

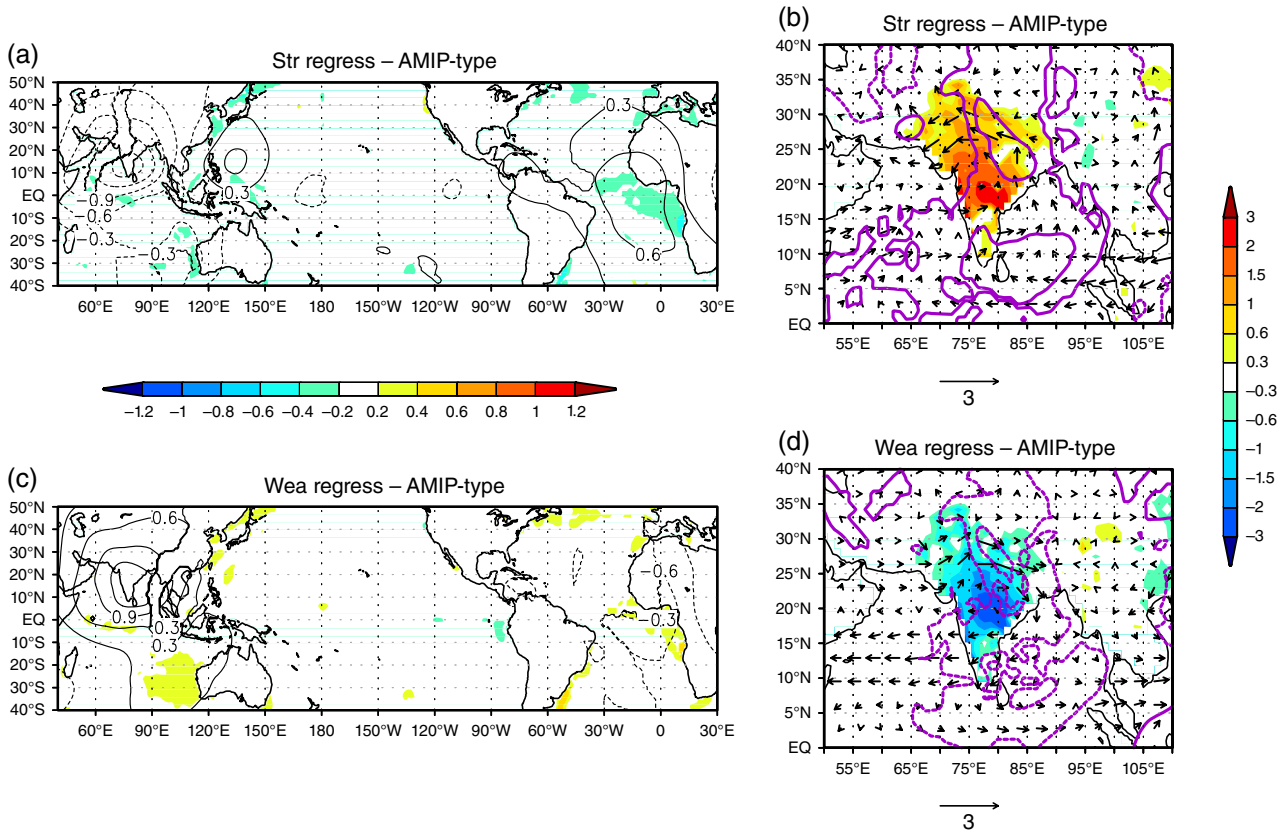

Figure 9. Anomalies of (a, c) SST (K, shaded) and velocity potential (*1.e-6 1/s2, contours) at 200 hPa and of (b,d) precipitation (mm/day, shaded), 850 hPa winds (m s^{-1}, vectors) and meridional wind shear (m s^{-1}, purple contours) removing the ENSO impact via linear regression according to Equation (1) for strong and weak monsoon years composite, respectively, in AMIP experiments. All the values shown are statistically significant at 95%.

is stronger than in the mean and a central eastern Pacific anomalously warm when the monsoon is weaker than in the mean. For the other cases shown in Figures 4(b) and (d), i.e. when the AMIP members have the monsoon index opposite to what observed, there are interesting similarities/differences between simulated strong and weak monsoon years. In fact, when the model simulates a weak monsoon instead of the observed strong one (Figure 4(b)), the SST in the Pacific Ocean is slightly positive with negative anomalies in the north-eastern (about 150°W, 40°N) and south-western (about 180°E, 20°S) sectors. This SST pattern recalls the warm ENSO phase and even if the anomalies in the eastern Pacific are not large, they are positive and associated with negative anomalies north and south, and with positive anomalies in the Indian Ocean. Surface temperature gradients in the Pacific Ocean are found to be effective for the ENSO teleconnections (Vera *et al.,* 2004). In the Indian Ocean, the SST pattern recalls the IOD mode in its positive phase and it is associated with a weak monsoon, differently from what expected (Ashok *et al.,* 2004). Because of the nature of the experiments used, i.e. AGCM with prescribed SST, we cannot expect the correct signal in the Indian Ocean where the crucial role of ocean–atmosphere coupling is well documented (Wu and Kirtman, 2004; Prodhomme *et al.,* 2014). Apart from the Pacific Ocean, large negative anomalies are located in the eastern Atlantic Ocean (Figure 4(b)).

The cases where the AMIP members have a strong monsoon instead of the observed weak one have slightly warm SST anomalies in the equatorial Pacific, and slightly cold SST anomalies in the North Atlantic, in the Western Pacific warm pool region and in the subtropical south-eastern Indian Ocean (Figure 4(d)). The comparison of the SST pattern in Figures 4(c) and (d) suggests that the forcing from other regions than the eastern Pacific alone may largely affect the intensity of the ISM rainfall. The analysis of specific cases in the next section helps further to better understand the characteristics of the remote forcing on the monsoon.

Figure 5 summarizes the relationship between monsoon precipitation index and Walker and local Hadley circulations in the AMIP members. In particular, for all the ensemble members the intensity of the standardized monsoon indices is related with an SLP index representing the intensity of the Walker circulation (Figure 5(a)) and with an index representing the intensity of the local Hadley circulation (Figure 5(b)). The intensity of the Walker circulation is measured with the difference in sea-level pressure (ΔSLP) between the central east Pacific (160°–80°W, 5°S–5°N) and the Indian Ocean/West Pacific sector (80°–160°E, 5°S–5°N), as defined by Vecchi *et al.* (2006). While the index of the local Hadley circulation has been computed as vertical meridional wind shear (i.e. v850 minus v200) averaged in 70°–110°E,

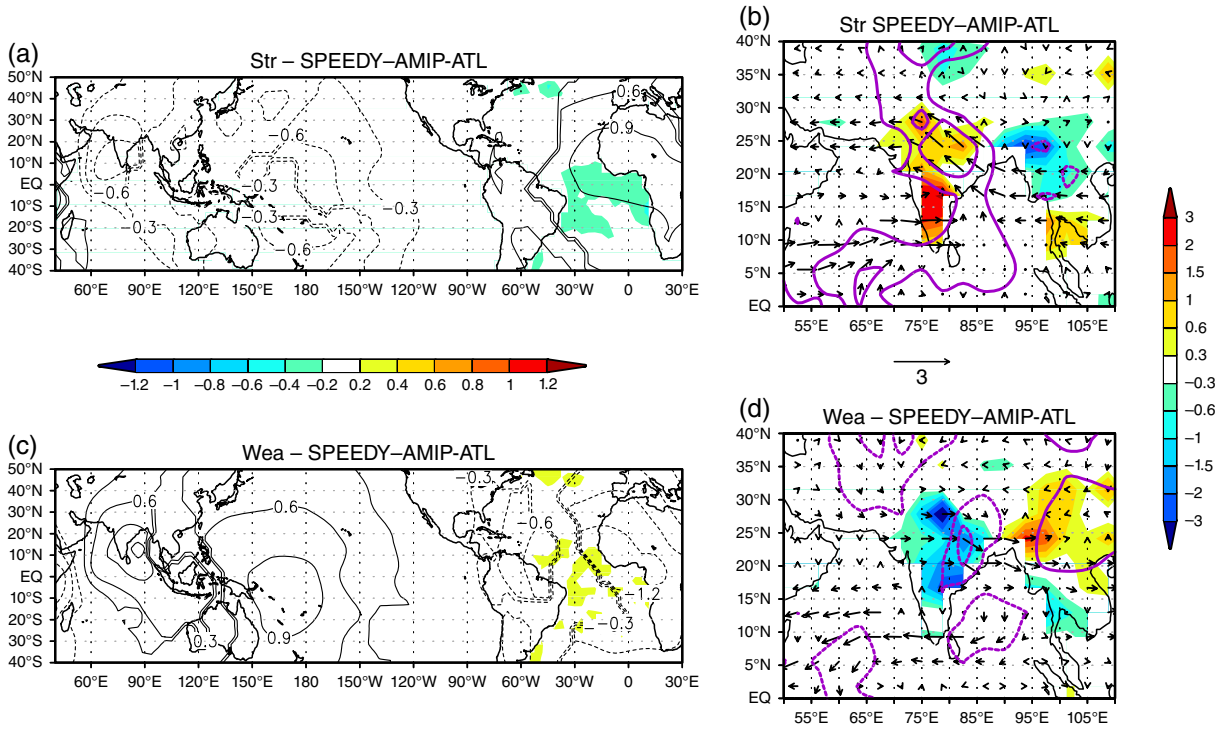

Figure 10. Anomalies of (a, c) SST (K, shaded) and velocity potential (*1.e^{-6} 1 s^{-2}, contours) at 200 hPa and of (b,d) precipitation (mm/day, shaded), 850 hPa winds (m s^{-1}, vectors) and meridional wind shear (m s^{-1}, purple contours) for strong and weak monsoon years composite, respectively, in the SPEEDY-AMIP-ATL ensemble (where prescribed SST is interannually varying only in the Atlantic while climatological in the rest of the ocean). All the values shown are statistically significant at 95%.

10°–30°N following the monsoon-Hadley (MH) index defined by Goswami *et al.* (1999).

In Figure 5(a), the values of the indices are scattered in the monsoon-Walker circulation space, with strong and weak monsoon years that are not exactly associated with strong and weak Walker circulation intensities, consistently with the non-univocal relationship between monsoon and ENSO. Nevertheless, the strong monsoon years in phase with the observations (blue plus signs) tend to have a positive and strong (i.e. larger than 1 standard deviation) ΔSLP index indicative of a stronger Walker circulation. The relationship is less neat in the case of weak monsoon years in phase with the observations (green filled squares), as some of them have a ΔSLP index largely negative, some have small negative values and a few have positive values. Instead, the relationship between the monsoon intensity and the intensity of the local Hadley circulation is clear and quasi-linear (Figure 5(b)), suggesting a tight link. But the intensity of the MH index is not necessarily large for strong and weak monsoon years, except for a few of them exceeding 1 standard deviation (either in the positive or negative *y*-axis). Similarly, there are more weak 'In Phase' monsoon years with large negative MH index (green filled squares) than the reverse (Figure 5(b)).

4. Analysis of specific years with common characteristics among the AMIP members

Following from the classification described in Section 2.3 and the results above, we focus now on three groups of years: (1) strong and weak monsoon years when at least half of the AMIP members are In Phase with the observations ('common In Phase') in Section 4.1, (2) strong and weak monsoon years when at least half of the AMIP members are out of phase with the observations ('common Out of Phase') in Section 4.2 and (3) strong and weak monsoon years in the AMIP that do not correspond to extreme years in the observations ('AMIP-only') in Section 4.3. The years grouped into these three classes are listed in Table 3.

4.1. Strong and weak monsoon years in phase with the observations ('common In Phase')

Figure 6 shows the anomalies of SST, 200 hPa velocity potential, precipitation, 850 hPa wind and meridional wind shear for strong and weak monsoon years composites for the ensemble members having the simulated ISM index in phase with the observations in at least half of the members (Table 3, second column). The patterns of SST in AMIP and HadISST are the same because the years considered in simulated and observed composites are the same (slight differences may be present and they are due to the fact that in the model we applied a statistical significance test so some values, likely the smaller ones, are masked out), but the response in the atmosphere differs because of the model biases and because of the lack of ocean–atmosphere coupling.

For the strong monsoon cases selected, the SST pattern is characterized by La Nina signature with negative anomalies in the eastern equatorial Pacific and positive

anomalies in the western North Pacific (Figures 6(a) and (c)). Actually, the two years classified into this group (i.e. 1961, 1970, see Table 3) do not share exactly the same characteristics: 1970 is a La Nina year while 1961 is not, likely because the negative anomalies are too small (not shown). For the rest of the ocean, small negative SST anomalies are located in the south Atlantic and eastern Indian Ocean (Figures 6(a) and (c)). The response in the atmosphere in terms of upper tropospheric velocity potential differs in the model and in the observations, specifically in the Pacific Ocean, but in both cases negative anomalies are located over South Asia and western Indian Ocean (Figures 6(a) and (c)). The effects over India are increased precipitation over the continent associated with enhanced south-westerly flow and increased meridional wind shear in the eastern Indian Ocean extending toward the continent (Figures 6(b) and (d)). This result is in line with the tight link between meridional wind shear and monsoon previously discussed in Figure 5(b).

For the weak monsoon years selected, the SST pattern has a strong El Nino signature with large positive SST anomalies in the eastern equatorial Pacific but also in the Indian Ocean and in the south Atlantic, with negative anomalies in the North Pacific (Figures 6(e) and (g)). In this case, the response in the atmosphere in terms of upper tropospheric velocity potential is quite similar with large negative anomalies in the Pacific sector, extending to South America, and large positive anomalies over South Asia with maxima over India and west of Australia (Figures 6(e) and (g)). The response over India is characterized by decreased precipitation over the continent and decreased south westerly flow, associated with negative meridional wind shear all over the region (Figures 6(f) and (h)). In this case, we may conclude that El Nino forcing is mostly responsible for the pattern over India, in fact the years selected in this case (i.e. 1987, 2002 and 2009, see Table 3) are all strong El Nino years. In particular, 1987 has been identified as a large predictable year also in a previous work using the same set of experiments (Cherchi and Navarra, 2013).

In terms of SST patterns, these cases do not differ much from the composites shown in Figure 4. The main difference is that the anomalies are a bit more intense, in line with the idea that specific cases are selected. However, even if in both cases the monsoon is classified as extreme compared to the mean, the circulation and precipitation patterns in the model differ from the observations. In particular, in the model the excess/deficit of precipitation is mostly localized south of 20°N (Figures 6(d) and (h)), while in CRU the maxima are north of 20°N and in the Western Ghats when the monsoon is strong (Figure 6(b)) and in the west at about 25°N when the monsoon is weak (Figure 6(f)). These differences are perfectly consistent with the differences in the lower-tropospheric winds, i.e. in the model they are straight westerlies/easterlies (Figures 6(d) and (h)), and the associated vertical shear in the observations has more north/south anomalies (Figures 6(b) and (f)).

4.2. Strong and weak monsoon years out of phase with the observations ('common Out of Phase')

The cases considered in this section are opposite to the ones of the previous section, as here the years analysed are classified as strong (weak) monsoon years according to the observations but are exactly in the opposite phase in the ensemble members, where they are classified as weak (strong) monsoon years in at least half of the members (Table 3, third column). According to this, the signature that we will describe over India will be exactly opposite, and we want to understand what is the origin of this difference and if it can be inferred to the SST forcing.

In the AMIP ensemble, one year (i.e. 1994, see Table 3) is classified as weak monsoon year despite it corresponds to a strong monsoon year in the observations. The SST pattern in that year (Figures 7(a) and (c)) is characterized by negative SST anomalies in the eastern equatorial Pacific Ocean and in the south western Pacific but positive SST anomalies in the central-western Pacific Ocean extending to the subtropics. In the Indian Ocean, the SST are negative in the east and slightly positive in the west, corresponding to a classical positive IOD pattern. In fact, 1994 is classified as IOD year (Meyers *et al.,* 2007; Ummenhofer *et al.,* 2009). In the Atlantic Ocean, the SST is slightly negative in the east along the equator, and it is largely negative in the north-eastern sector, with a positive anomaly in the west close to the American coast (Figures 7(a) and (c)). The velocity potential pattern in the upper troposphere associated to these SST anomalies differs in the model and in the observations. In fact, in the observations negative velocity potential anomalies cover the eastern Pacific and the American continent, and negative anomalies as well cover the South Asian sector, implying positive precipitation over the Indian subcontinent (Figure 7(b)), with positive meridional wind shear over the continent and negative over the Indian Ocean in the west. On the other hand, in the AMIP members the velocity potential anomalies are negative all over the Pacific Ocean, but they are positive over South Asia (Figure 7(c)), associated with negative precipitation anomalies over India and negative meridional wind shear (Figure 7(d)). Following also from the interpretation of Figure 4, the lack of ocean–atmosphere coupling over the eastern Indian Ocean may be the key to explain the differences. In fact, in the observations the presence of a positive IOD in the Indian Ocean induces convergence and precipitation over India because of the air-sea processes at work (Ashok *et al.,* 2004). On the other hand, in our experimental setup the response over India in terms of precipitation and circulation is directly linked to the SST forcing from the positive SST anomalies in the central Pacific Ocean and the Walker circulation shifts, in line with the theory from Kumar *et al.* (2006).

For the cases classified as weak monsoon years in the observations but simulated as strong monsoon years in the AMIP members (i.e. 1974, 1979, see Table 3), the SSTs are characterized by weak negative anomalies in the central Pacific and strong negative anomalies in the North Atlantic Ocean (Figures 7(e) and (g)). Despite this, the response in the upper tropospheric velocity potential is

opposite in the model and in the observations: in fact in the observations it is negative in the eastern Pacific Ocean and over the Atlantic and it is positive over the Asian continent and western Pacific, while in the model it is negative over Asia (with a maximum over India) and positive in the Atlantic Ocean (Figures 7(e) and (g)). The local response over India is characterized by negative (positive) precipitation over India in the observations (model), associated with weaker (stronger) south-westerly flow and negative (positive) meridional wind shear (Figures 7(f) and (h)). As for the case described before, here we can speculate that in the AMIP members the response over India is mostly related with the negative SST anomalies in the Pacific and associated Walker circulation, while in the observations other effects (including ocean–atmosphere coupling processes) could have played a more effective role.

4.3. Strong and weak monsoon years in AMIP members only ('AMIP-only')

The last case is dedicated to those years that are classified as strong or weak monsoon years in most of the AMIP members (at least in half of them) but not in the observations (Table 3, fourth column). In this case, strong monsoon years in AMIP are 1955, 1958 and 1978 (Table 3), and they are all characterized by negative anomalies in the eastern equatorial Pacific, the Indian Ocean and the eastern south Atlantic (Figures 8(a) and (c)). Probably the anomalies in the Pacific Ocean are too weak to be classified as La Nina or they do not last up to the following winter, but they are large enough in summer to modulate the Walker circulation and provide large convection over South Asia (Figures 8(c) and (d)). The anomalies of velocity potential at 200 hPa differ in sign over the Pacific and Atlantic Oceans, but they agree over the Asian continent (Figures 8(a) and (c)), and the response over India is characterized by intense precipitation in the continent, slightly enhanced south-westerly flow and positive meridional wind shear (Figures 8(b) and (d)).

On the other hand, years that are classified as weak monsoon in the majority of AMIP members are 1990, 1991, 1993 and 1995 (Table 3), but none of them is classified as weak monsoon year in the observations. In the AMIP in fact, in these years the composite of the precipitation over India is largely negative with a weaker south-westerly flow and intense weak meridional wind shear (Figure 8(h)), while in the observations despite a weaker south-westerly flow and a strong negative meridional wind shear the precipitation anomalies are close to zero or slightly positive (Figure 8(f)). In both cases, the velocity potential anomalies over India are positive (but in AMIP the intensity is larger), and they differ in the Pacific and Atlantic basins (Figures 8(e) and (g)). The SST pattern beneath is characterized by positive anomalies in the central Pacific and in the Indian Ocean, while in the other basins the anomalies are close to zero (Figures 8(e) and (g)). In particular, the warm SST anomalies in the central Indian Ocean recalls the structure of the extreme drought of 2008 as described in Rao *et al.* (2010). These two cases have the clear SST signature of ENSO also in the Indian Ocean, suggesting that the intensity of the monsoon is a response to the forcing from the ocean and from ENSO in particular.

4.4. Implications for non-ENSO forcing

The correlation between NINO3.4 and precipitation over India is about −0.61 (in the record 1948–2012), meaning that about 40% of the monsoon variability is related to ENSO and meaning also that there is another 60% of variability that is related to something else, like forcing from other sectors (but ENSO influences also SST in places different from the tropical Pacific) or the internal variability. In our AMIP experiments, the correlation coefficient is smaller (−0.36) and we have discussed in the manuscript aspects of the SST forcing and lacking of ocean–atmosphere coupling able to explain and understand that difference.

As described in Section 2.4 using Equation (1), we remove the ENSO signal through regression processes from SST and other atmospheric fields anomalies in the AMIP ensemble. These regressed fields anomalies are then used to build composites for strong and weak monsoon years (Figure 9). When ENSO signal is removed, extreme monsoon conditions are associated with anomalies in the tropical Atlantic and in small areas of the eastern North Atlantic and south Indian Ocean. In particular, excess monsoon rainfall is linked with small negative SST anomalies in the equatorial Atlantic Ocean close to Africa and in the south Indian Ocean close to Australia (Figure 9(a)). In the South Atlantic and south Indian Ocean, the anomalies are of opposite sign for extreme deficit monsoon rainfall (Figure 9(c)). Similar results can be seen applying the same regression exercise to the observations (not shown). The region in the Atlantic Ocean where the anomalies are larger corresponds to the area identified in Kucharski *et al.* (2007) as modulating the interdecadal variability of the ENSO-monsoon relationship.

To support the value of the results for the Atlantic Ocean, we include the analysis of two sets of AMIP experiments performed with the SPEEDY atmospheric model, as described in Section 2.4, comparing strong and weak monsoon composites when the interannual variability of the global ocean is prescribed and when the interannual variability is prescribed only in the Atlantic Ocean (SPEEDY-AMIP-ATL) while the rest of the SST is climatological. The experimental setup mimic the non-ENSO fields described above but it does not have the limitation of the technique applied. Figure 10 shows the composites of the ensemble of AMIP experiments performed with SPEEDY and identified as SPEEDY-AMIP-ATL. The results are perfectly in line with the results of Figure 9, where ENSO was linearly removed. A shortcoming for these sets of experiments is that in SPEEDY the ENSO-monsoon connection is not well captured, actually it is weak and it has the opposite sign (not shown). Such a behaviour in the SPEEDY model has been reported in a multi-model AGCM assessment and is also observed in some other AGCMs (Kucharski *et al.,* 2009b). It is related

to excessive influences from Indian Ocean SST anomalies that co-vary with ENSO. On the other hand, a correct tropical Atlantic-monsoon relationship has been reported in Kucharski *et al.* (2008, 2009a).

5. Conclusions

An ensemble of AMIP-type experiments with prescribed interannual varying SST and different initial conditions is used to study the relationship between ISM extreme conditions and ENSO. In this study, we intend to contribute to the understanding of the ENSO-monsoon relationship with emphasis on the characteristics of the remote forcing from the Pacific Ocean but also from the other basins, like Indian and Atlantic Oceans. At first, we select strong and weak monsoon years in an ensemble of eight AMIP experiments sharing the same SST and sea-ice boundary conditions for the period 1948–2012 and with different initial conditions. Then, another classification is performed selecting years where the model index peaks in phase with the observations and years where the indices peaks are exactly opposite thus building 'In Phase' and 'Out of Phase' groups. Considering the eight members available, relative large samples of cases can be built, ensuring also the statistical significance of the patterns shown.

Considering 'In Phase' composites, the SST pattern is clearly in ENSO phase with an eastern equatorial Pacific Ocean anomalously cold when the monsoon is stronger than in the mean and a central eastern Pacific anomalously warm when the monsoon is weaker than in the mean. When the AMIP members have the monsoon index opposite to what observed, there are interesting similarities/differences between simulated strong and weak monsoon years. In terms of winds, especially in the weak 'Out of Phase' case the flow has a larger southerly component confined east of 65°E and entering the continent mostly from south, compared to the strong 'In Phase' composite.

The comparison of 'In Phase' and 'Out of Phase' composites reveals the importance of the ocean–atmosphere coupling in modulating the influence of ENSO on convection over India. In particular, in our AMIP composites a positive IOD pattern together with El Nino is associated with deficit of precipitation over India. The explanation relies on the lack of ocean–atmosphere coupling processes in our experimental setup, crucial for the region in those cases.

From all the cases analysed, it appears that in terms of SST forcing the classical ENSO pattern with anomalies of the same sign in the tropical Pacific Ocean but also in the Indian and Atlantic tropical sectors is a clear common characteristic of extreme monsoon years. The SST pattern in summer seems enough to modulate the Walker circulation and consequently suppress or enhance convection over South Asia, even if it does not evolve into an ENSO event.

Once the signature from ENSO is removed, the region in the Atlantic Ocean where the anomalies are larger corresponds to the area identified in Kucharski *et al.* (2007) as modulating the interdecadal variability of the ENSO-monsoon relationship. These results are confirmed also by the composite of strong and weak monsoon years in an ensemble of AMIP experiments performed with the SPEEDY atmospheric model where interannually varying SST are prescribed only in the Atlantic Ocean. The forcing from other regions than the eastern Pacific alone may largely affect the intensity of the ISM rainfall.

In this study, the simple approach of linearly removing ENSO did not allow a full understanding of the role of non-ENSO forcing. Forthcoming research using specific monsoon protocol experiments with state of the art coupled models (i.e. Global Monsoon Model Intercomparison Project (GMMIP) within next CMIP6) is planned and it will permit to investigate the role of forcing from the different basins but also to better exploit the role of ocean–atmosphere coupling, crucial to fully understand the ISM variability.

Acknowledgements

We are grateful to the reviewers for their valuable work.

References

Annamalai H, Liu P. 2005. Response of the Asian summer monsoon to changes in el Nino properties. *Q. J. R. Meteorol Soc* **131**: 805–831.
Annamalai H, Hamilton K, Sperber K. 2007. The South Asian summer monsoon and its relationship with ENSO in the IPCC AR4 simulations. *J. Clim.* **20**: 1071–1092.
Annamalai H, Hafner J, Sooraj KP, Pillai P. 2013. Global warming shifts the monsoon circulation drying South Asia. *J. Clim.* **26**: 2701–2718.
Ashok K, Guan Z, Yamagata T. 2001. Impact of the Indian Ocean dipole on the relationship between the Indian monsoon rainfall and ENSO. *Geophys. Res. Lett.* **28**: 4499–4502.
Ashok K, Guan Z, Saji NH, Yamagata T. 2004. Individual and combined influences of ENSO and the Indian Ocean Dipole on the Indian summer monsoon. *J. Clim.* **17**: 3141–3155.
Barimalala R, Bracco A, Kucharski F. 2012. The representation of the south tropical Atlantic teleconnection to the Indian Ocean in the AR4 coupled models. *Clim. Dyn.* **38**(5–6): 1147–1166. https://doi.org/10.1007/s00382-011-1082-5.
Charney JG, Shukla J. 1981. Predictability of monsoons. In *Monsoon Dynamics*, Lighthill J, Pearce RP (eds). Cambridge University Press: Cambridge, UK, 99–108.
Chen H, Schneider EK. 2014. Comparison of the SST-forced response between coupled and uncoupled climate simulations. *J. Clim.* **27**: 740–756.
Cherchi A, Navarra A. 2007. Sensitivity of the Asian summer monsoon to the horizontal resolution: differences between AMIP-type and coupled model experiments. *Clim. Dyn.* **28**: 273–290.
Cherchi A, Navarra A. 2013. Influence of ENSO and of the Indian Ocean dipole on the Indian summer monsoon variability. *Clim. Dyn.* **41**: 81–103. https://doi.org/10.1007/s00382-012-1602-y.
Cherchi A, Carril AF, Menendez CG, Zamboni L. 2014. La Plata basin precipitation variability in spring: role of remote SST forcing as simulated by GCM experiments. *Clim. Dyn.* **42**: 219–236.
Cobb KM, Charles CD, Cheng H, Edwards RL. 2003. El Nino southern oscillation and tropical Pacific climate during the last millennium. *Nature* **424**: 271–276.
Cobb KM, Westphal N, Sayani HR, Watson JT, Di Lorenzo E, Cheng H, Edwards R, Charles CD. 2013. Highly variable el Nino southern oscillation throughout the Holocene. *Science* **339**: 67–70.
Collins M, An SI, Cai W, Ganachaud A, Guilyardi E, Jin FF, Jochum M, Lengaigne M, Power S, Timmermann A, Vecchi G, Wittenberg A. 2010. The impact of global warming on the tropical Pacific Ocean and El Nino. *Nat. Geosci.* **3**: 391–397.
Compo G, Sardeshmukh P. 2010. Removing ENSO-related variations from the climate records. *J. Clim.* **23**: 1957–1978.

Fasullo J, Webster PJ. 2002. Hydrological signatures relating the Asian summer monsoon and ENSO. *J. Clim.* **15**: 3082–3095.
Fennessy MJ, Kinter JL III, Kirtman B, Marx L, Nigam S, Schneider E, Shukla J, Straus D, Vernekar A, Xue Y, Zhou J. 1994. The simulated Indian monsoon: a GCM sensitivity study. *J. Clim.* **7**: 33–43.
Gernushov A, Schneider N, Barnett T. 2001. Low frequency modulation of the ENSO-Indian monsoon rainfall relationship: signal or noise? *J. Clim.* **14**: 2486–2492.
Goswami BN. 1994. Dynamic predictability of seasonal monsoon rainfall: problems and prospects. *Proc. Indian Acad. Sci.* **60A**: 101–120.
Goswami BN. 1998. Interannual variations of Indian summer monsoon in a GCM: external conditions versus internal feedbacks. *J. Clim.* **11**: 501–521.
Goswami BN, Xavier PK. 2005. Dynamics of internal interannual variability of the Indian summer monsoon in a GCM. *J. Geophys. Res.* **110**: D24104.
Goswami BN, Krishnamurthy V, Annamalai H. 1999. A broad-scale circulation index for the interannual variability of the Indian summer monsoon. *Q. J. R. Meteorol. Soc.* **125**: 611–633.
Jourdain NC, Gupta A, Taschetto AS, Ummenhofer CC, Moise AF, Ashok K. 2013. The Indo-Australian monsoon and its relationship to ENSO and IOD in re-analysis and the CMIP3/CMIP5 simulations. *Clim. Dyn.* **41**: 3073–3102. https://doi.org/10.1007/s00382-013-1676-1.
Kalnay E, Kanamitsu M, Kistler R, Collins W, Deaven D, Gandin L, Iredell M, Saha S, White G, Woollen J, Zhu Y, Leetmaa A, Reynolds R. 1996. The NCEP/NCAR 40-year reanalysis project. *Bull. Am. Meteorol. Soc.* **77**: 437–471.
Kinter JL III, Miyakoda K, Yang S. 2002. Recent changes in the connection from the Asian monsoon to ENSO. *J. Clim.* **15**: 1203–1215.
Kirtman BP, Shukla J. 2000. Influence of the Indian summer monsoon on ENSO. *Q. J. R. Meteorol. Soc.* **126**: 213–239.
Kosaka Y, Xie SP. 2013. Recent global-warming hiatus tied to equatorial Pacific surface cooling. *Nature* **501**: 403–407.
Krishnamurthy V, Goswami BN. 2000. Indian monsoon-ENSO relationship on interdecadal timescale. *J. Clim.* **13**: 579–595.
Krishnamurthy L, Krishnamurthy V. 2014. Influence of PDO on South Asian summer monsoon and monsoon-ENSO relation. *Clim. Dyn.* **42**: 2397–2410. https://doi.org/10.1007/s00382-013-1856-z.
Krishnan R, Sabin TP, Ayantika TC, Kitoh A, Sugi M, Murakami H, Turner AG, Slingo JM, Rajendran K. 2012. Will the South Asian monsoon overturning circulation stabilize any further? *Clim. Dyn.* **40**: 187–211.
Kucharski F, Joshi MK. 2017. Influence of tropical South Atlantic Sea surface temperatures on the Indian summer monsoon in CMIP5 models. *Q. J. R. Meteorol. Soc.* **143**: 1351–1363.
Kucharski F, Bracco A, Yoo JH, Molteni F. 2007. Low-frequency variability of the Indian monsoon-ENSO relationship and the tropical Atlantic: the "weakening" of the 1980s and 1990s. *J. Clim.* **20**: 4255–4266.
Kucharski F, Bracco A, Yoo JH, Molteni F. 2008. Atlantic forced component of the Indian monsoon interannual variability. *Geophys. Res. Lett.* **35**: L04706. https://doi.org/10.1029/2007GL033037.
Kucharski F, Bracco A, Yoo JH, Tompkins AM, Feudale L, Ruti P. 2009a. A Gill-Matsuno-type mechanism explains the tropical Atlantic influence on African and Indian monsoon rainfall. *Q. J. R. Meteorol. Soc.* **579**: 569–579. https://doi.org/10.1002/qj.
Kucharski F, Scaife A A, Yoo J H, Folland C K, Kinter J, Knight J, Fereday D, Fischer A M, Jin E K, Kröger J, Lau N-C, Nakaegawa T, Nath M J, Pegion P, Rozanov E, Schubert S, Sporyshev P V, Syktus J, Voldoire A, Yoon J H, Zeng N, Zhou T, Kucharski F, Scaife A A. 2009b. The CLIVAR C20C project: skill of simulating Indian monsoon rainfall on interannual to decadal timescales. Does GHG forcing play a role? *Clim. Dyn.* **33**: 615–627. https://doi.org/10.1007/s00382-008-0462-y.
Kucharski F, Kang IS, Farneti R, Feudale L. 2011. Tropical Pacific response to 20th century Atlantic warming. *Geophys. Res. Lett.* **38**: L03702. https://doi.org/10.1029/2010GL046248.
Kucharski F, Molteni F, King MP, Farneti R, Kang IS, Feudale L. 2013. On the Need of Intermediate Complexity General Circulation Models: A "SPEEDY" Example. *Bull. Am. Meteorol. Soc.* **94**: 25–30.
Kumar KK, Rajagopalan B, Kane MA. 1999. On the weakening relationship between the Indian monsoon and ENSO. *Science* **284**: 2156–2159.
Kumar KK, Rajagopalan B, Hoerling M, Bates G, Cane M. 2006. Unraveling the mystery of Indian monsoon failure during el Nino. *Science* **314**: 115–119.
Lau NC, Nath MJ. 2000. Impact of ENSO on the variability of the Asian-Australian monsoon as simulated in GCM experiments. *J. Clim.* **13**: 4287–4309.
Li J, Xie SP, Cook ER, Huang G, D'Arrigo R, Liu F, Ma J, Zheng XT. 2011. Interdecadal modulation of El Nino amplitude during the past millennium. *Nat. Clim. Change* **1**: 114–118.
Losada T, Rodriguez-Fonseca B, Polo I, Janicot S, Gervois S, Chauvin F, Ruti P. 2010. Tropical response to the Atlantic Equatorial mode: AGCM multimodel approach. *Clim. Dyn.* **35**: 45–52. https://doi.org/10.1007/s00382-009-0624-6.
Luo JJ, Sasakia W, Masumoto Y. 2012. Indian Ocean warming modulates Pacific climate change. *Proc. Nat. Acad. Sci. USA* **109**: 18701–18706. https://doi.org/10.1073/pnas.1210239109.
McGregor S, Timmermann A, Stuecker MF, England MH, Merrifield M, Jin FF, Chikamoto Y. 2014. Recent Walker circulation strengthening and Pacific cooling amplified by Atlantic warming. *Nat. Clim. Change* **4**: 888–892. https://doi.org/10.1038/nclimate2330.
Meyers GA, McIntosh PC, Pigot L, Pook MJ. 2007. The years of El Nino, La Nina and interactions with the tropical Indian Ocean. *J. Clim.* **20**: 2872–2880.
Mitchell TD, Jones PD. 2005. An improved method of constructing a database of monthly climate observations and associated high-resolution grids. *Int. J. Climatol.* **25**: 693–712.
Mohan RSA, Goswami BN. 2003. Potential predictability of the Asian summer monsoon on monthly and seasonal time scales. *Meteorol. Atmos. Phys.* **84**: 83–100.
van Oldenborgh GJ, Burgers G. 2005. Searching for decadal variations in ENSO precipitation teleconnections. *Geophys. Res. Lett.* **32**: L15701.
Park JS, Yeh SW, Kug JS. 2012. Revisited relationship between tropical and North Pacific sea surface temperature variations. *Geophys. Res. Lett.* **39**: L02703. https://doi.org/10.1029/2011GL050005.
Parthasarathy B, Munot AA, Kothwale DR. 1992. Indian summer monsoon rainfall indices: 1871–1990. *Meteorol. Mag.* **121**: 174–186.
Pottapinjara V, Girishkumar MS, Ravichandran M, Murtugudde R. 2014. Influence of the Atlantic zonal mode on monsoon depressions in the Bay of Bengal during boreal summer. *J. Geophys. Res. Atmos.* **119**(11): 6456–6469. https://doi.org/10.1002/2014JD021494.
Pottapinjara V, Girishkumar MS, Sivareddy S, Ravichandran, Murtugudde R. 2016. Relation between the upper ocean heat content in the equatorial Atlantic during boreal spring and the Indian monsoon rainfall during June-September. *Int. J. Climatol.* **36**: 2469–2480. https://doi.org/10.1002/joc.4506.
Prodhomme C, Terray P, Masson S, Izumo T, Tozuka T, Yamagata T. 2014. Impact of Indian Ocean SST biases on the Indian monsoon as simulated in a global coupled model. *Clim. Dyn.* **42**: 271–290. https://doi.org/10.1007/s00382-013-1671-6.
Prodhomme C, Terray P, Masson S, Boschat G, Izumo T. 2015. Ocean factors controlling the Indian summer monsoon onset in a coupled model. *Clim. Dyn.* **44**: 977–1002.
Rao SA, Chaudhari HS, Pokhrel S, Goswami BN. 2010. Unusual central Indian drought of summer monsoon 2008: role of southern tropical Indian Ocean warming. *J. Clim.* **23**: 5163–5174.
Rasmusson EM, Carpenter TH. 1983. The relationship between eastern equatorial Pacific sea surface temperature and rainfall over India and Sri Lanka. *Mon. Weather Rev.* **111**: 517–528.
Ratna SB, Cherchi A, Joseph PV, Behera SK, Abish B, Masina S. 2016. Moisture variability over the indo-Pacific region and its influence on the Indian summer monsoon rainfall. *Clim. Dyn.* **46**: 949–965.
Rayner NA, Parker DE, Horton EB, Folland CK, Alexander LV, Rowell DP, Kent EC, Kaplan A. 2003. Global analysis of sea surface temperature, sea ice and night marine air temperature since the late nineteenth century. *J. Geophys. Res.* **18**(D14): 4407. https://doi.org/10.1029/2002JD002670.
Roeckner E, Arpe K, Bengtsson L, Christoph M, Claussen M, Dümenil L, Esch M, Giorgetta M, Schlese U, Schulzweida U. 1996. The Atmospheric general circulation Model ECHAM4: Model description and simulation of present-day climate. Report No. 218, Max-Planck Institut fur Meteorologie, Hamburg, Germany.
Shukla J. 1981. Dynamical predictability of monthly means. *J. Atmos. Sci.* **38**: 2547–2572.
Shukla J. 1984. Predictability of time averages: part II. The influence of the boundary forcing. In *Problems and Prospects in Long and Medium Range Weather Forecasting*, Burridge DM, Kallen E (eds). Springer: Berlin Heidelberg, 155–206.
Sikka DR. 1980. Some aspects of the large-scale fluctuations of summer monsoon rainfall over India in relations to fluctuations in the planetary and regional scale circulation parameter. *Proc. Indian Acad. Sci.* **89**: 179–195.

Singh SV, Kriplani RH. 1986. Potential predictability of lower-tropospheric monsoon circulation and rainfall over India. *Mon. Weather Rev.* **114**: 758–763.

Sohn BJ, Yeh SW, Schmetz J, Song HJ. 2013. Observational evidences of Walker circulation change over the last 30 years contrasting with GCM results. *Clim. Dyn.* **40**: 1721–1732. https://doi.org/10.1007/s00382-012-1484-z.

Sperber KR. 1999. Are revised models better models? A skill score assessment of regional inter-annual variability. *Geophys. Res. Lett.* **26**: 1267–1270.

Sperber KR, Palmer TN. 1996. Interannual tropical rainfall variability in general circulation model simulations associated with the atmospheric model intercomparison project. *J. Clim.* **9**: 2727–2750.

Sperber KR, Slingo J, Annamalai H. 2000. Predictability and relationship between sub-seasonal and interannual variability during the Asian summer monsoons. *Q. J. R. Meteorol. Soc.* **126**: 2545–2574.

Sperber KR, Annamalai H, Kang IS, Kitoh A, Moise A, Turner A, Wang B, Zhou T. 2013. The Asian summer monsoon: an intercomparison of CMIP5 vs CMIP3 simulations on the late 20th century. *Clim. Dyn.* **41**: 2711–2744. https://doi.org/10.1007/s00382-012-1607-6.

Taylor KE, Stouffer RJ, Meehl GA. 2011. An overview of CMIP5 and the experiment design. *Bull. Am. Meteorol Soc.* **93**: 485–498.

Torrence C, Webster PJ. 1999. Interdecadal changes in the ENSO-monsoon system. *J. Clim.* **12**: 2679–2690.

Trenberth KE, Hurrell JW. 1994. Decadal atmosphere-ocean variations in the Pacific. *Clim. Dyn.* **9**: 303–319.

Turner AG, Annamalai H. 2012. Climate change and the South Asian summer monsoon. *Nat. Clim. Change* **2**: 1–9.

Ummenhofer CC, England MH, McIntosh PC, Meyers GA, Pook MJ, Risbey JS, Sen Gupta A, Taschetto AS. 2009. What causes southeast Australia's worst droughts? *Geophys. Res. Lett.* **36**: L04706. https://doi.org/10.1029/2008GL036801.

Vecchi GA, Soden BJ, Wittenberg AT, Held IM, Leetmaa A, Harrison MJ. 2006. Weakening of tropical Pacific atmospheric circulation due to anthropogenic forcing. *Nature* **441**: 73–76. https://doi.org/10.1038/nature04744.

Vera C, Silvestri G, Barros V, Carril A. 2004. Differences in El Nino response over the Southern Hemisphere. *J. Clim.* **17**(9): 1741–1753.

Vimont D, Battisti DS, Hirst AC. 2001. Footprinting: a seasonal connection between the tropics and mid-latitudes. *Geophys. Res. Lett.* **28**: 3923–3926.

Vimont D, Wallace JM, Battisti DS. 2003. The seasonal footprinting mechanism in the Pacific: implications for ENSO. *J. Clim.* **16**: 2668–2675.

Walker GT. 1924. Correlation in seasonal variations of weather, IX: a further study of world weather. *VIII Mem. India Meteorol. Dept.* **24**: 275–332.

Wang B, Liu J, Kim HJ, Webster PJ, Yim SY. 2012. Recent change of the global monsoon precipitation (1979-2008). *Clim. Dyn.* **39**: 1123–1135. https://doi.org/10.1007/s00382-011-1266-z.

Wang B, Liu J, Kim HJ, Webster PJ, Yim SY, Xiang BQ. 2013. Northern Hemisphere summer monsoon intensified by mega-El Nino/Southern Oscillation and Atlantic Multidecadal Oscillation. *Proc. Natl. Acad. Sci. USA.* **110**: 5347–5352. https://doi.org/10.1073/pnas.1219405110.

Webster P, Hoyos CD. 2010. Beyond the spring barrier? *Nat. Geosci.* **3**: 152–153.

Webster PJ, Magana V, Palmer TN, Shukla J, Tomas RA, Yanai M, Yasunari T. 1998. Monsoons: processes, predictability and the prospects for prediction. *J. Geophys. Res.* **103**, **451–14**(510): 14.

Wilks DS. 1995. *Statistical Methods in the Atmospheric Sciences*. Academic Press: London, 467.

Wu R, Kirtman BP. 2004. Impacts of Indian Ocean on the Indian summer monsoon-ENSO relationship. *J. Clim.* **17**: 3037–3054.

Xavier PK, Marzin C, Goswami BN. 2007. An objective definition of the Indian summer monsoon season and a new perspective on the ENSO-monsoon relationship. *Q. J. R. Meteorol. Soc.* **133**: 749–764.

Yadav RK. 2017. On the relationship between east equatorial Atlantic SST and ISM through Eurasian wave. *Clim. Dyn.* **48**: 281–295. https://doi.org/10.1007/s00382-016-3074-y.

